

Article

Vertical Distribution and Mineralization Dynamics of Organic Carbon in Soil and Its Aggregates in the Chinese Loess Plateau Driven by Precipitation

Chunyang Gao ¹, Zhidan Zhang ^{1,*}, Meijia Li ¹, Bohan Feng ¹, Yipeng Zhou ¹, Jinjing Zhang ^{1,*} and Nianpeng He ^{2,*}

¹ College of Resources and Environmental Science, Jilin Agricultural University, Changchun 130117, China; 18946737450@163.com (C.G.); limeijia19990123@163.com (M.L.); fengbohan77@163.com (B.F.); yipengzhou95@163.com (Y.Z.)

² Key Laboratory of Sustainable Forest Ecosystem Management-Ministry of Education, Northeast Forestry University, Harbin 150040, China

* Correspondence: zhidanzhang79@163.com (Z.Z.); zhangjinjing@126.com (J.Z.); henp@igsnr.ac.cn (N.H.)

Abstract: The mineralization of soil organic carbon (SOC) is a critical process in the soil carbon cycle. This study aimed to investigate the vertical distribution characteristics and mineralization dynamics of SOC in soils and their aggregates across different steppe types in the Loess Plateau (LP). Soil profiles from three steppe types under varying precipitation gradients were selected: meadow steppe (MS), typical steppe (TS), and desert steppe (DS). A 60-day controlled laboratory incubation study was conducted for carbon mineralization and the influence of climatic and soil properties on SOC mineralization was analyzed. The results showed that the SOC content and cumulative mineralization (C_M) in 1–2 mm aggregates were higher than in other particle sizes; SOC content and C_M followed the order MS > TS > DS and both decreased significantly with increasing soil depth. Correlation analysis revealed that precipitation significantly affected aggregate mineralization ($p < 0.001$) and that mineralization in the 1–2 mm aggregates was more closely related to mean annual precipitation (MAP), SOC, and water-soluble organic carbon (SWOC). Precipitation primarily controlled SOC mineralization in the 0–50 cm soil layer, while SOC mineralization in the 50–100 cm layer was influenced by soil-related carbon content. Structural Equation Modeling indicated that precipitation influences the mineralization of organic carbon in topsoil indirectly through its direct impact on SOC. In the context of global warming, the SOC turnover rate in high-precipitation areas (MS) was faster than in low-precipitation areas (TS, DS), necessitating greater attention to soil carbon dynamics in these regions.

Keywords: Loess Plateau; precipitation impact; soil aggregate; soil organic carbon content; accumulated mineralization amount



Citation: Gao, C.; Zhang, Z.; Li, M.; Feng, B.; Zhou, Y.; Zhang, J.; He, N. Vertical Distribution and Mineralization Dynamics of Organic Carbon in Soil and Its Aggregates in the Chinese Loess Plateau Driven by Precipitation. *Appl. Sci.* **2024**, *14*, 3852. <https://doi.org/10.3390/app14093852>

Academic Editor: Paola Grenni

Received: 11 April 2024

Revised: 26 April 2024

Accepted: 28 April 2024

Published: 30 April 2024



Copyright: © 2024 by the authors. Licensee MDPI, Basel, Switzerland. This article is an open access article distributed under the terms and conditions of the Creative Commons Attribution (CC BY) license (<https://creativecommons.org/licenses/by/4.0/>).

1. Introduction

In recent years, global climate change has emerged as a significant environmental issue. Soil is pivotal in controlling the global carbon cycle, serving as the largest carbon reservoir in the terrestrial biosphere [1]. It is estimated that 1500 Pg C is stored in soils as organic matter, three times that in the atmosphere or terrestrial vegetation [2,3]. Consequently, even minor variations in SOC content can profoundly impact the concentration of carbon dioxide (CO₂) in the atmosphere [4]. In this context, research on the stability of SOC has become a focal point in scientific studies. Studies indicated that water is a fundamental driver for nearly all chemical and biological processes, including plant growth and survival, photosynthesis, microbial activity, and soil respiration [5]. Based on this, precipitation is considered a primary factor affecting SOC inputs, with different precipitation patterns significantly impacting the function and structure of terrestrial ecosystems. A meta-analysis of precipitation manipulation experiments showed that increased precipitation stimulates

soil respiration by an average of 30%, while reduced precipitation decreases it by 12% [6]. Soil aggregates, as the main reservoirs of SOC, provide physical protection for SOC and are crucial for carbon sequestration [7,8]. Alternating wet–dry and freeze–thaw cycles, driven by precipitation and temperature, were primary factors affecting aggregate stability [9–11] and the stability of soil aggregates was vital for maintaining ecosystem functions.

It is well-known that surface soils contain a substantial amount of organic carbon, which can be rapidly decomposed and transformed by microorganisms, releasing CO₂ into the atmosphere [12]. However, it is estimated that over 50% of soil carbon is located in subsoil (below 30 cm), where the carbon dynamics may significantly differ from those in the topsoil [13]. For instance, deep soil layers were more susceptible to nutrient inputs and temperature increases than the surface layers [14]. Yet, in soil carbon dynamics research, subsoil studies are sparse and this aspect of soil organic carbon mineralization has been overlooked often. Additionally, the factors influencing carbon mineralization in topsoil and subsoil may differ and research into subsoil carbon mineralization could make a significant contribution to reducing atmospheric carbon in the context of global climate change [15,16]. Overall, the vertical distribution patterns and regulatory factors of soil protection present significant research value.

The mineralization of organic carbon is a vital biogeochemical process occurring naturally in soil, crucial for maintaining soil fertility, nutrient release, mitigating greenhouse gas emissions, and impacting global climate change. The mineralization of organic carbon is influenced by factors such as the quality of SOC and biological elements like microorganisms, both of which are indirectly controlled by abiotic factors like temperature and precipitation [17,18]. Soil aggregates also play a vital role in the decomposition of SOC. Studies have shown that factors influencing the formation of aggregates also affect the mineralization of SOC [19]. The physical protection ability of soil aggregates for SOC varies with the particle size of aggregates. This highlights the necessity of considering soil structure when predicting future SOC dynamic trajectories. The steppe soils of the Loess Plateau have garnered attention due to their crucial role in China's national carbon budget. Steppe ecosystems, with substantial organic carbon storage, are susceptible to global climate change. The Loess Plateau is located in central China and is the largest concentrated area of loess distribution in China. It falls within the temperate monsoon climate zone, with the eastern and southern parts being characterized by a warm temperate semi-humid monsoon climate, while the northwest part experiences a temperate semi-humid monsoon climate. The soils in this region are predominantly loess and the vegetation is primarily composed of grasslands, shrubs, and a small amount of deciduous broad-leaved forests. To date, studies on soil mineralization in natural steppe profiles in the Loess Plateau region have been relatively scarce. Previous research had primarily focused on surface soils of farmlands, steppes, and artificial forests. Therefore, further research on profile soils and their aggregates under natural conditions can enhance our understanding of carbon sequestration dynamics. Understanding the factors influencing SOC and its aggregate mineralization dynamics in natural steppes under varying precipitation gradients is vital for comprehending the carbon balance of natural steppe ecosystems and more accurately predicting their response to climate change. We had hypothesized whether, in regions with high precipitation, the soil's organic carbon content and accumulated mineralization might increase, leading to a potential acceleration in its turnover rate. With this in mind, the objectives of this study are to (1) investigate the patterns of SOC and its aggregate mineralization in soil profiles of three types of steppes along precipitation gradients in the Loess Plateau region of China; (2) analyze the factors influencing SOC and its aggregate mineralization; and (3) better evaluate the relationships between SOC mineralization, climate, and soil properties.

2. Materials and Methods

2.1. Experimental Area

This study was conducted in three types of steppes in the Loess Plateau, which were distributed along a precipitation gradient from west to east (Figure 1). Ten sites were

selected, including meadow steppe (S1, S2, and S3), typical steppe (S4, S5, S6, and S7), and desert steppe (S8, S9, and S10). The transect spanned approximately 800 km, with altitudes ranging from 804 to 1714 m. The mean annual temperature (MAT) varies between 7.71 and 11.85 °C and the MAP ranges from 215.50 to 591.18 mm (Table 1). The environmental variations along the precipitation gradient of the Loess Plateau provided a living laboratory for studying the relationship between soil and its aggregate organic carbon mineralization under natural environmental conditions. The MAT and MAP data were sourced from the National Earth System Science Data Center, National Science and Technology Infrastructure of China, 2018 (<http://www.geodata.cn/main/#/> accessed date 26 April 2024).

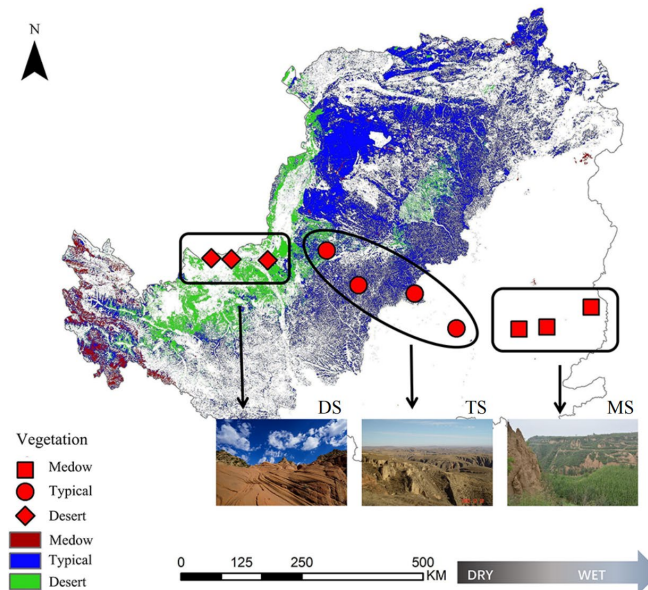


Figure 1. Spatial distribution of sampling points of different steppes types in the Loess Plateau. Field sampling along the east–west precipitation gradient was covered with meadow steppe (square: S1, S2, and S3), typical steppe (round: S4, S5, and S6), and desert steppe (diamond: S7, S8, and S9).

Table 1. Basic information on the study sites.

Number	Steppe Type	Latitude	Longitude	Altitude (m)	MAP (mm)	MAT (°C)	pH
01	MS	N 44°35′43.244″	E 113°21′23.256″	792	563.88	11.85	8.08
02	MS	N 44°35′43.245″	E 112°17′36.672″	879	591.18	9.96	7.95
03	MS	N 44°35′43.246″	E 111°38′05.172″	832	566.12	10.66	8.12
04	TS	N 44°35′43.247″	E 110°10′53.256″	915	533.36	10.72	8.08
05	TS	N 44°35′43.248″	E 109°15′11.052″	1325	498.89	9.50	8.17
06	TS	N 44°35′43.249″	E 107°55′17.112″	1382	438.09	7.46	8.03
07	TS	N 44°35′43.250″	E 107°11′12.876″	1545	395.14	5.23	8.07
08	DS	N 44°35′43.251″	E 105°46′37.812″	1309	320.35	5.87	8.15
09	DS	N 44°35′43.252″	E 104°35′43.008″	1684	233.88	7.56	8.09
10	DS	N 44°35′43.253″	E 104°26′38.580″	1666	215.5	7.71	8.43

MS: meadow steppe; TS: typical steppe; DS: desert steppe; MAT and MAP: mean annual temperature and precipitation.

2.2. Soil Sampling

Soil samples were collected in early August 2018. At each site, we randomly established four plots (1 m × 1 m). After removing surface litter, soil samples from 0 to 100 cm depth were collected using a soil auger in the four plots spaced 100 m apart. The soil samples were sieved, manually cleared of roots and visible organic debris, passed through a 10 mm sieve, air-dried for a week, and stored for future use.

2.3. Sample Preparation and Analysis

The distribution of aggregates was determined using dry and wet sieving methods. Initially, 300 g of soil sample was shaken for 3 min on an electric vibratory sieve to obtain aggregates of eight sizes: 7–10, 5–7, 3–5, 2–3, 1–2, 0.5–1, 0.25–0.5, and <0.25 mm [20]. The components were weighed to determine their proportion in the total dry soil sample weight. The separated samples were then combined into a composite soil and 50 g of this recombined composite soil was placed on a sieving machine (LM12-XSB-88, Zhetai Machinery Manufacturing Co., Shanghai, China) equipped with 2 mm, 1 mm, 0.5 mm, 0.25 mm, and 0.053 mm sieves. The samples were soaked in deionized water at room temperature for 10 min. Subsequently, the sieves were vibrated 250 times for 10 min with an amplitude of 30 mm. This process yielded aggregates of five sizes (>2 mm, 1–2 mm, 0.5–1 mm, 0.25–0.5 mm, 0.053–0.25 mm, and <0.053 mm). The aggregates were then dried to a constant weight in a 60 °C dryer and weighed [21].

The POC was determined using hexametaphosphate extractions [22]. The SOC was measured using the $K_2Cr_2O_7$ oxidation method [23]. Soil bulk density (BD) was determined using the undisturbed core method. A subsample from each sampling location was dried at 105 °C to a constant mass and used to determine the remaining moisture for bulk density calculations. A laser-diffraction particle-size analyzer (Mastersizer, 2000, Malvern, UK) was used to divide the soil into clay (<2 µm), silt (2–20 µm), and sand (20–2000 µm), according to the international soil texture classification standard. Soil pH was determined using a pH meter (MYRON L Ultrameter II™, Carlsbad, CA, USA) [24].

The mean weight diameter (MWD) was used as an indicator to characterize the structure of large soil aggregates, calculated using the formula

$$MWD = \sum_{i=1}^n X_i W_i \quad (1)$$

where W_i is the percentage weight of the sample on the sieves used for analysis and X_i is the mean diameter of aggregate size classes (mm) [25].

2.4. Incubation Experiment

One gram each of undisturbed profile soil samples (0–10 cm, 10–30 cm, 30–50 cm, and 50–100 cm) and dry-sieved samples (3–5 mm, 1–2 mm, and 0.25–0.5 mm) along with wet-sieved samples (1–2 mm, 0.25–0.5 mm, and <0.053 mm) were taken. Then, 0.6 mL of distilled water was added to achieve a moisture content of 60% (w/w) and placed the samples in 30 mL test tubes with lids for incubation at 25 °C. The CO_2 concentration was measured as follows: the test tubes were sealed at time 0, 9 mL of air was injected into the tubes, and 9 mL of gas was extracted and injected it into a glass vacuum tube containing 5.8 mL of CO_2 -absorbing solution, serving as the CO_2 concentration at day 0 (d-0). After 1 day, 9 mL of gas from the test tubes was extracted and injected it into a glass vacuum tube containing 5.8 mL of CO_2 -absorbing solution as the CO_2 concentration at day 1 (d-1). Subsequently, the incubation tube cap was opened to achieve gas equilibrium with the indoor environment before sealing it again. The same procedures were repeated on days 2, 3, 5, 7, 10, 15, 20, 25, 30, 35, 40, 45, 50, 55, and 60. Gas samples were analyzed using an Agilent 7820A gas chromatograph (Agilent Technologies, Carpinteria, CA, USA). The evolution of carbon dioxide was calculated based on Robertson (1999) [26].

The formula for calculating the SOC mineralization process is

$$C_M = C_o(1 - e^{-kt}) \quad (2)$$

where C_M ($mg\ kg^{-1}$) is the cumulative amount of carbon dioxide released over different intervals (days); C_o is the carbon that can be mineralized without time limitation; and k is the first-order rate constant (d^{-1}) [25].

2.5. Statistical Analysis

All treatments were replicated three times. Data analysis and graphing were completed using SPSS 26.0 and Origin 2021. Pearson (Origin 2021) correlation analysis was used to analyze the relationship between climatic factors and soil organic carbon mineralization. Redundancy Analysis (RDA) was employed to determine the factors influencing SOC mineralization and their relative contributions to this variation (Canoco 5.0). The response mechanism of SOC mineralization to environmental gradients was determined using Structural Equation Modeling (SEM) (SPSS Amos v22.0). The fit of this SEM model was evaluated using the χ^2 test, degrees of freedom (df), and *p*-value. Spatial analysis was conducted using ESRI ArcGIS (Redlands Institute of Environmental Systems, Redlands, CA, USA).

3. Results

3.1. Particle Size Distribution of Soil Aggregates

In the TS and DS steppe types, the proportion of aggregates smaller than 0.25 mm was the highest, accounting for 49.36% (TS) to 51.74% (DS). In contrast, the proportion of aggregates smaller than 0.25 mm in MS was significantly lower than in TS and DS. MS was predominantly comprised 1–2 mm aggregates, accounting for 20.25% of the total (Figure 2). The proportions of 1–2 mm, 0.5–1 mm, and 0.25–0.5 mm aggregates showed a noticeable decline with the decrease in the precipitation gradient, in the order of MS > TS > DS. Overall, MS had a higher proportion of larger aggregates, while TS and DS had higher proportions of smaller aggregates.

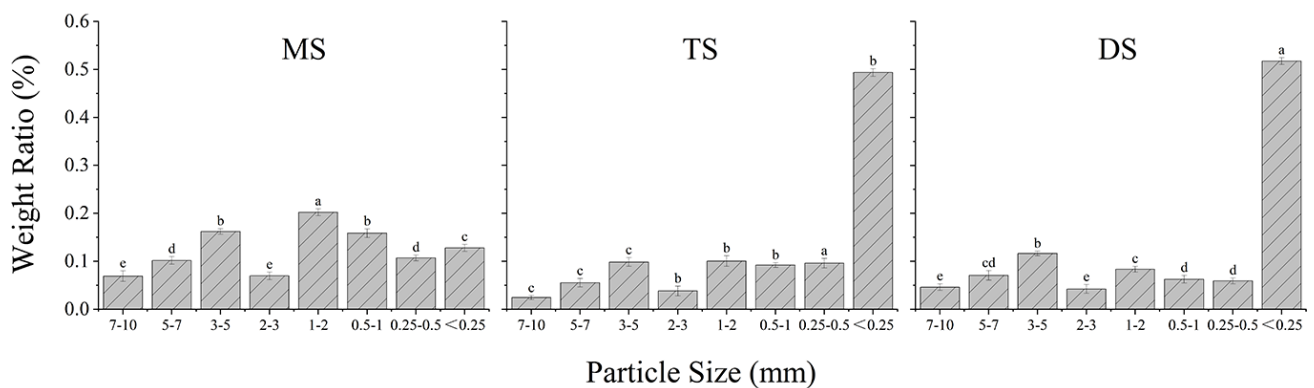


Figure 2. Soil aggregate distribution of different steppe types in the Loess Plateau. Different letters indicate significant differences between the three grassland types, $p < 0.05$. MS: meadow steppe; TS: typical steppe; DS: desert steppe.

3.2. Soil Profile and Aggregate Organic Carbon Content

3.2.1. Variations in SOC and C_M in Soil Profiles

Figure 3 illustrates the variations in SOC and C_M across different steppe types in soil profiles of the Loess Plateau. Overall, both SOC content and C_M showed a declining trend with the decrease in the precipitation gradient, with MS being significantly higher than TS and TS being significantly higher than DS. Furthermore, within the same steppe type, SOC and C_M exhibited a decreasing trend with increasing soil profile depth. Under MS conditions, the SOC contents at soil depths of 0–10 cm are 20.89 g kg^{-1} , which were 43.97% higher than this under TS conditions. Compared to DS conditions, the value was 155.07% higher. It indicated that the decrease in precipitation gradient significantly affected SOC content and consequently, the cumulative mineralization of organic carbon.

3.2.2. Soil Aggregate Organic Carbon Content

Figure 4 displayed the organic carbon content of soil aggregates in three types of steppes on the plateau. Regardless of whether they were mechanical or water-stable soil aggregates, MS significantly exceeded other steppe types in organic carbon content. There was an apparent decline in soil aggregate organic carbon content with the decrease in the

precipitation gradient, with MS been considerably higher than TS and significantly higher than DS. For example, in MS, the organic carbon contents of mechanical aggregates of 1–2 mm is 23.33 g kg⁻¹, which were 16.77% higher than this in TS and 71.92% higher than in DS. When comparing the organic carbon contents of different sizes of aggregates within the same steppe type, we found that 1–2 mm size aggregates had higher organic carbon content. For example, in MS mechanical aggregates, the 1–2 mm particle size contained 5.90% more organic carbon than the 3–5 mm size and 25.16% more than the 0.25–0.5 mm size. When comparing mechanical and water-stable soil aggregates, we found that for the same steppe type and particle size, the organic carbon content was consistently higher in mechanical aggregates than in water-stable aggregates.

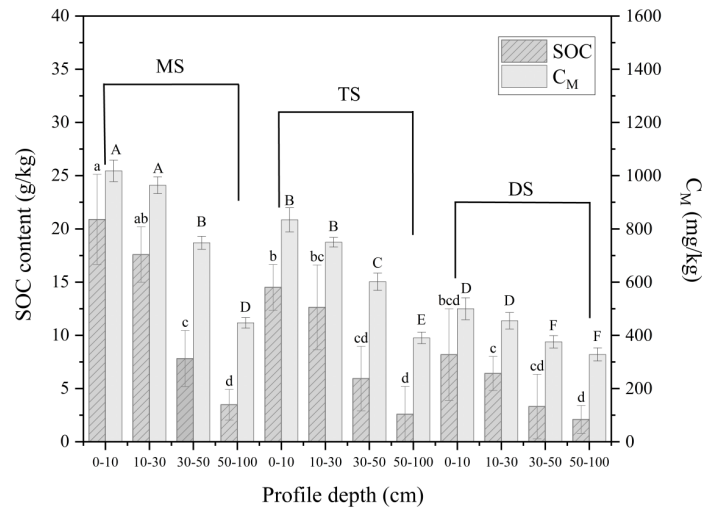


Figure 3. SOC and C_M of the Loess Plateau section vary with steppe type. Bars represent the standard error. Different letters indicate a significant difference between steppe types ($p < 0.05$). Lowercase letters indicate SOC groups and uppercase letters indicate C_M groups. MS: meadow steppe; TS: typical steppe; DS: desert steppe.

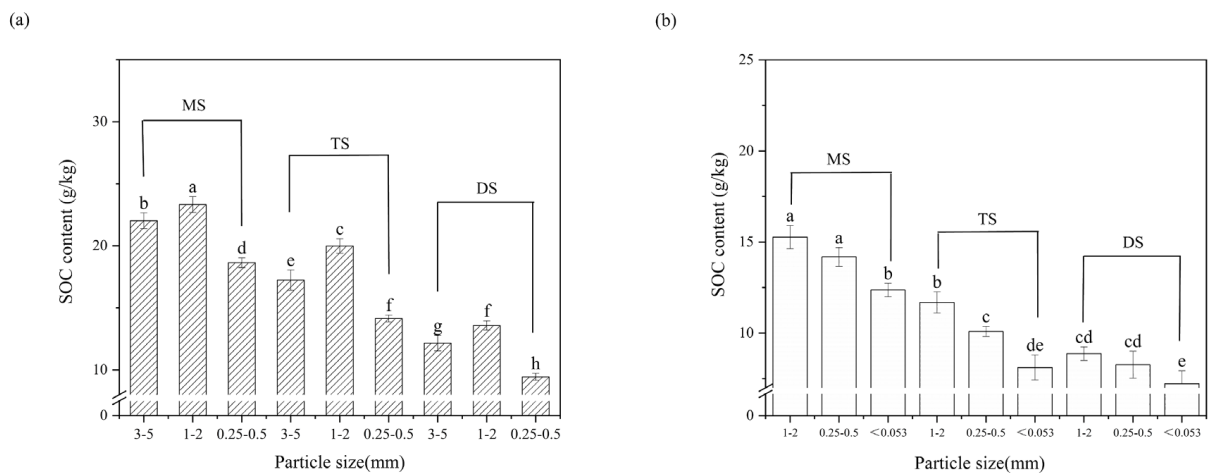


Figure 4. SOC content of soil aggregates of the three steppe types in the Loess Plateau. (a) Mechanical aggregates and (b) water-stable aggregates. Bars represent the standard error. Different letters represent a significant difference between steppe types ($p < 0.05$). MS: meadow steppe; TS: typical steppe; DS: desert steppe.

3.3. Mineralization Dynamics

3.3.1. Mineralization Dynamics of Soil Profiles

Figure 5 illustrates the variations in CO₂ emission and cumulative mineralization of soil profiles across three types of steppes over the incubation period. Within the 60-day

incubation period, the order of soil organic carbon mineralization and cumulative mineralization among the steppe types was as follows: MS > TS > DS. Taking the 0–10 cm soil layer as an example, the cumulative mineralization amounts for the three steppe types were MS (1018.15 mg kg⁻¹), TS (834.03 mg kg⁻¹), and DS (499.86 mg kg⁻¹). CO₂ emissions were initially rapid at the beginning of the incubation but gradually decreased over time. In the initial phase, the mineralization amounts for MS and TS were much higher than for DS. In the later stage from 10 to 60 days, the decreasing trend slowed down and then stabilized. The highest cumulative mineralization in the three steppe types was in MS (0–10) at 1018.15 mg kg⁻¹, while the lowest was in DS (50–100) at 328.16 mg kg⁻¹.

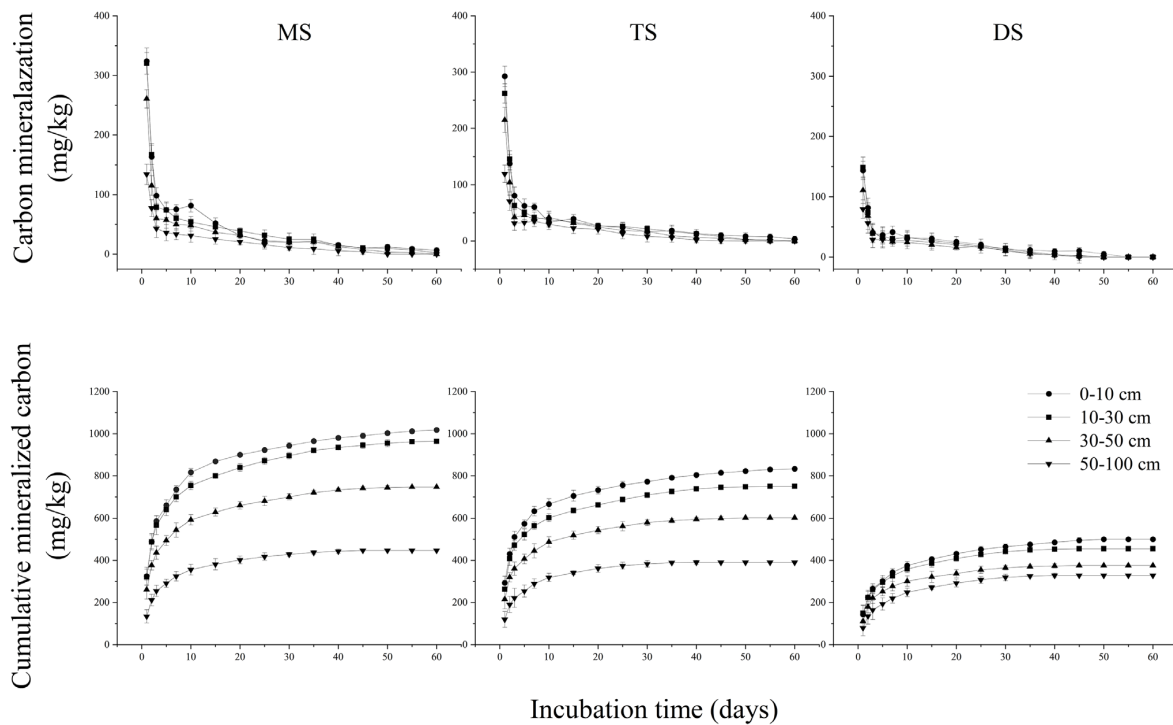


Figure 5. Dynamics and cumulative mineralization of SOC in the Loess Plateau profile. MS: meadow steppe; TS: typical steppe; DS: desert steppe.

In this study, SOC mineralization followed first-order kinetics, as only labile carbon was mineralized during the 60-day incubation period. Curve fitting parameters, as shown in Table 1, indicated that the turnover rate coefficient k was highest for MS and lowest for DS. The potential mineralizable carbon (C_0) was highest for MS at 939.14 mg kg⁻¹ and lowest for DS at 446.28 mg kg⁻¹ (Table 2).

Table 2. Dynamic parameters of SOC mineralization process in the Loess Plateau profile.

Steppe-Types	Fitting Parameters		
	C_0 (mg C kg ⁻¹)	K (d ⁻¹)	R^2
MS	939.14 ± 19.43 a	0.31 ± 0.03 a	0.94
TS	775.49 ± 16.52 b	0.26 ± 0.04 b	0.91
DS	469.66 ± 11.30 c	0.20 ± 0.03 c	0.92

Different letters indicate a significant difference between steppe types ($p < 0.05$). MS: meadow steppe; TS: typical steppe; DS: desert steppe; C_0 : potential carbon that could be mineralized without time limit; K : parameter of turnover coefficient; R^2 : fitting results.

3.3.2. Mineralization Dynamics of Soil Aggregates

Figures 6 and 7 depict the changes in CO₂ emission and cumulative mineralization of soil aggregates under three grassland types over the incubation time. Within the 60-day

incubation period, the order of mineralization and cumulative mineralization among different grassland types was MS > TS > DS. The mineralization patterns for different grassland types all exhibited a higher mineralization rate in the initial stage, with a rapid increase in cumulative mineralization. Specifically, the initial 0–10 days showed a faster mineralization rate, reaching a relatively stable state around day 40. Among the three grassland types, the mineralization and cumulative mineralization of different mechanical aggregate sizes were highest in 1–2 mm, followed by 3–5 mm, and lowest in 0.25–0.5 mm. For MS, the cumulative mineralization amounts were 1146.60 mg kg⁻¹, 1002.75 mg kg⁻¹, and 880.38 mg kg⁻¹, respectively. The mineralization rate and cumulative mineralization of different water-stable aggregate sizes were also highest in 1–2 mm, followed by 0.25–0.5 mm, and lowest in <0.053 mm, with MS showing cumulative mineralization amounts of 937.55 mg kg⁻¹, 848.31 mg kg⁻¹, and 800.49 mg kg⁻¹, respectively.

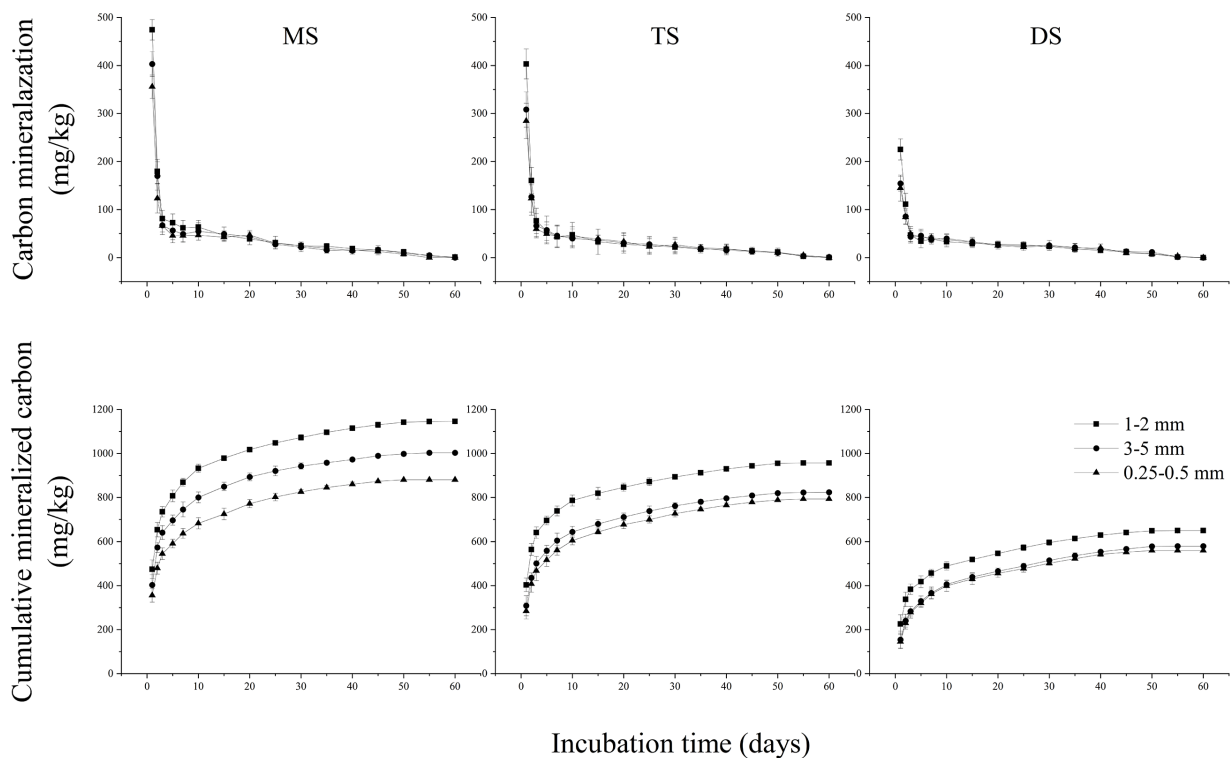


Figure 6. Dynamics and cumulative mineralization of SOC of mechanical aggregates in the Loess Plateau. MS: meadow steppe; TS: typical steppe; DS: desert steppe.

In this study, SOC mineralization followed first-order kinetics, as only labile carbon was mineralized during the 60-day incubation period. Curve fitting parameters, as shown in Tables 3 and 4, indicated that the turnover rate coefficient k was highest for MS. The potential mineralizable carbon (C_0) was highest for MS and lowest for DS.

Table 3. Dynamic parameters of the SOC mineralization process of mechanical aggregates in the Loess Plateau.

Steppe-Types	Particle Size (mm)	Fitting Parameters		
		C_0 (mg C kg ⁻¹)	K (d ⁻¹)	R^2
MS	1–2	1066.47 ± 25.28 a	0.39 ± 0.05 ab	0.83
	3–5	932.03 ± 23.11 b	0.38 ± 0.05 abc	0.82
	0.25–0.5	817.33 ± 26.37 d	0.34 ± 0.05 bc	0.80

Table 3. Cont.

Steppe-Types	Particle Size (mm)	Fitting Parameters		
		Co (mg C kg ⁻¹)	K (d ⁻¹)	R ²
TS	1–2	888.05 ± 20.20 c	0.43 ± 0.06 a	0.82
	3–5	761.06 ± 19.30 e	0.33 ± 0.04 bc	0.84
	0.25–0.5	729.86 ± 20.01 e	0.30 ± 0.04 c	0.83
DS	1–2	596.83 ± 17.21 f	0.30 ± 0.04 c	0.82
	3–5	533.67 ± 15.78 g	0.19 ± 0.03 d	0.88
	0.25–0.5	519.04 ± 14.44 g	0.20 ± 0.03 d	0.90

Different letters indicate a significant difference between steppe types ($p < 0.05$). MS: meadow steppe; TS: typical steppe; DS: desert steppe; Co: potential carbon that could be mineralized without time limit; K: parameter of turnover coefficient; R²: fitting results.

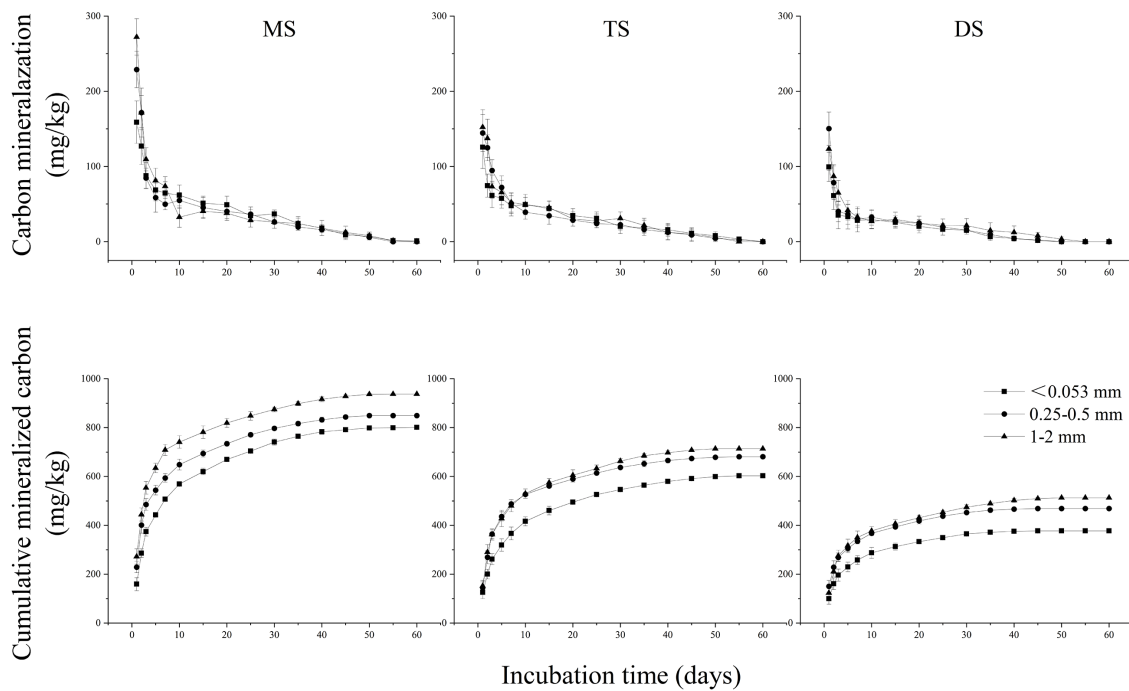


Figure 7. Dynamics and cumulative mineralization of SOC of water-stable aggregates in the Loess Plateau. MS: meadow steppe; TS: typical steppe; DS: desert steppe.

Table 4. Dynamic parameters of the SOC mineralization process of water-stable aggregates in the Loess Plateau.

Steppe-Types	Particle Size (mm)	Fitting Parameters		
		Co (mg C kg ⁻¹)	K (d ⁻¹)	R ²
MS	<0.053	759.32 ± 16.94 c	0.17 ± 0.02 ef	0.94
	0.25–0.5	798.23 ± 18.90 b	0.25 ± 0.03 abc	0.90
	1–2	880.18 ± 18.00 a	0.29 ± 0.03 a	0.92
TS	<0.053	568.93 ± 12.81 f	0.15 ± 0.02 f	0.95
	0.25–0.5	644.38 ± 11.94 e	0.22 ± 0.02 bcd	0.95
	1–2	673.94 ± 14.79 d	0.20 ± 0.02 de	0.93
DS	<0.053	362.32 ± 7.58 h	0.21 ± 0.02 cde	0.93
	0.25–0.5	466.56 ± 10.28 g	0.26 ± 0.03 ab	0.90
	1–2	480.99 ± 11.65 g	0.22 ± 0.02 bcd	0.91

Different letters indicate a significant difference between steppe types ($p < 0.05$). MS: meadow steppe; TS: typical steppe; DS: desert steppe; Co: potential carbon that could be mineralized without time limit; K: parameter of turnover coefficient; R²: fitting results.

3.4. Factors Influencing Soil Organic Carbon Mineralization

Overall, SOC mineralization in soil profiles showed significant positive correlations with MAP, SOC, POC, and SWOC ($p < 0.01$) and a significant negative correlation with elevation ($p < 0.05$) (Figure 8). However, it was observed that SOC mineralization in the 0–50 cm soil layer had a highly significant positive correlation with precipitation ($p < 0.001$), while the 50–100 cm soil layer was highly significantly correlated with SOC and POC ($p < 0.001$). It suggested that precipitation primarily controls SOC mineralization in the 0–50 cm soil layer, while the mineralization in the 50–100 cm layer was more closely related to soil-associated carbon. Notably, Clay + Silt showed a significant positive correlation with SOC mineralization in the 50–100 cm soil layer ($p < 0.05$) but no significant correlation with the 0–50 cm layer. The mineralization of organic carbon in soil aggregates exhibited a highly significant positive correlation with precipitation ($p < 0.001$), indicating that precipitation was a dominant factor affecting the mineralization of soil aggregates. Additionally, SOC and SWOC showed a highly significant positive correlation with the mineralization of 1–2 mm diameter soil aggregates ($p < 0.001$) and POC was significantly positively correlated with the mineralization of all sizes of soil aggregates ($p < 0.05$), suggesting that soil-associated carbon is also a dominant factor in the mineralization of soil aggregates, with a particularly close relationship with 1–2 mm diameter aggregates.

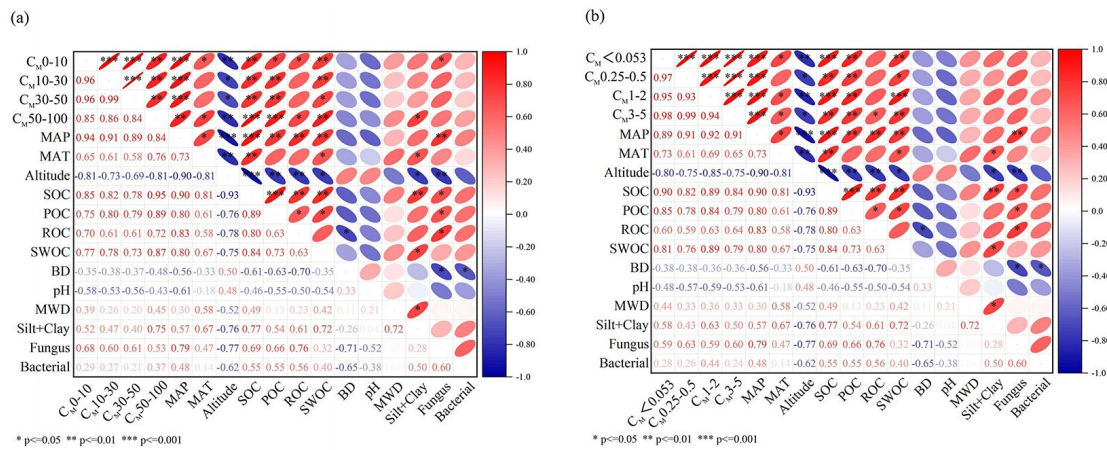


Figure 8. Correlation analysis between soil organic carbon mineralization in soil profiles (a) and soil aggregates (b) of the Loess Plateau and environmental and soil factors (* $p < 0.05$, ** $p < 0.01$, and *** $p < 0.001$). Blue indicates a positive correlation, while red indicates a negative correlation. MAP, mean annual precipitation; MAT, mean annual temperature; BD, bulk density; POC, particulate organic carbon; ROC, readily oxidizable carbon; SWOC, water-soluble organic carbon; MWD, mean weight diameter.

The results of Redundancy Analysis (RDA) (Figure 9) showed that the first and second axes explained 99.14% of the relationship between environmental factors and changes in soil organic carbon mineralization in the soil profiles of the Loess Plateau area (a). Among these, MAP was the primary factor influencing the spatial variation in soil organic carbon mineralization, accounting for 84.00% of the explanation ($p < 0.01$). The vectors of MAP, SOC, POC, and SWOC were quite long and the angles with C_M 0–10 cm, C_M 10–30 cm, C_M 30–50 cm, and C_M 50–100 cm were acute, indicating that these indicators had a strong positive impact on soil organic carbon mineralization. MAP and SOC had a greater influence on C_M 0–10 cm than on C_M 50–100 cm, whereas C_M 50–100 cm was more influenced by SOC and POC. Soil pH, elevation, and BD, with obtuse angles, had a negative impact. In Figure 9b, the first and second axes explained 99.14% of the relationship between environmental factors and changes in organic carbon mineralization of soil aggregates in the Loess Plateau area. Here, MAP was the main factor affecting the spatial variation in organic carbon mineralization in soil aggregates, explaining 83.00% ($p < 0.01$). The

mineralization of 1–2 mm aggregates was more closely related to MAP, SOC, POC, and SWOC, compared to other particle sizes.

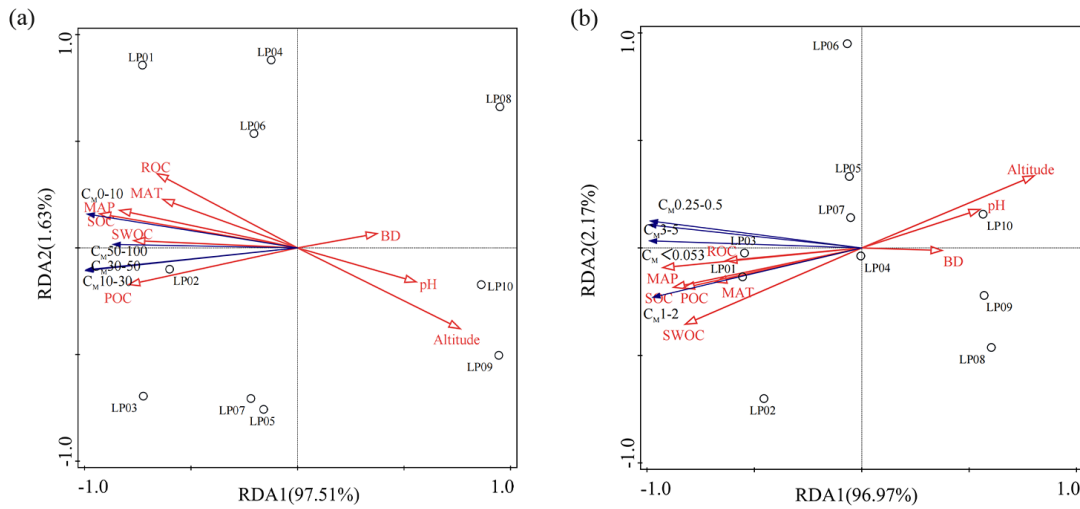


Figure 9. Biplot analysis constrained by environmental and soil factors and Redundancy Analysis (RDA) for soil organic carbon mineralization in soil profiles (a) and soil aggregates (b) of the Loess Plateau. Blue vectors represent soil organic carbon mineralization, while red vectors represent environmental and soil factors. The horizontal and vertical axes indicate loadings. MAP, mean annual precipitation; MAT, mean annual temperature; BD, bulk density; POC, particulate organic carbon; ROC, readily oxidizable carbon; SWOC, water-soluble organic carbon.

In the structural equation analysis, the model exhibited high fit ($\chi^2 = 4.023$, $df = 4.000$, $p = 0.403$, $rmsea = 0.025$) (Figure 10). The spatial variation in soil organic carbon was explained by 80.0%, with MAP having the most significant impact, with a factor coefficient of 0.89 ($p < 0.001$). The spatial variation in soil organic carbon mineralization in the 0–10 cm layer was 88.0%, with the most influential variable being MAP, followed by SOC ($p < 0.05$). For the 50–100 cm layer, the spatial variation in soil organic carbon mineralization was 77.0%, most influenced by Clay + Silt, followed by POC ($p < 0.05$). MAP primarily controlled the mineralization of SOC in the topsoil, indirectly affecting it through its direct impact on SOC. The mineralization in the subsoil was more closely associated with POC and Clay + Silt, with MAP also indirectly affecting this layer through its direct impact on POC.

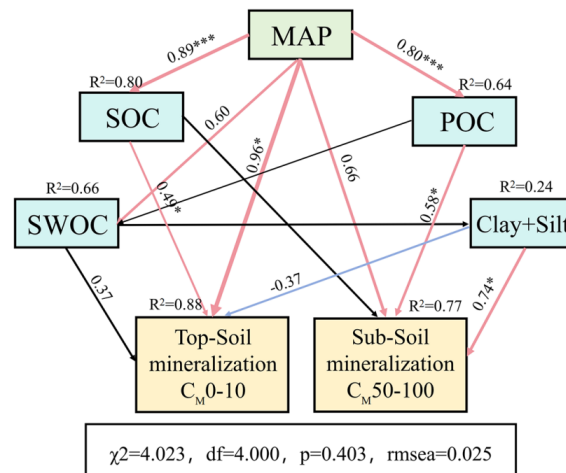


Figure 10. Results of the Structural Equation Model (SEM) for soil organic carbon mineralization, showing environmental and soil factors (* $p < 0.05$, *** $p < 0.001$). Solid blue arrows and solid red

arrows represent positive and negative correlations, respectively. The thickness of the path arrows reflected the strength of the relationship. The proportion of variance explained (R^2) appears next to each response variable in the model. The goodness-of-fit statistics for this model were as indicated in the SEM model. MAP, mean annual precipitation; POC, particulate organic carbon; SWOC, water-soluble organic carbon.

4. Discussion

4.1. Carbon Storage and Mineralization in Soil Aggregates

Differences in environmental factors such as dry–wet and freeze–thaw cycles led to variations in aggregate formation and the stability of soil aggregates along the precipitation gradient. Regions with a more humid climate and higher temperatures were conducive to the formation and stabilization of macro-aggregates. Soil aggregates are the fundamental units of soil structure and their quantity and quality determine the physicochemical properties and coherence of the soil. In this study, the 1–2, 0.5–1, and 0.25–0.5 mm aggregate fractions decreased with a reduction in the precipitation gradient. In comparison, the <0.25 mm aggregate fraction increased, indicating that precipitation is a significant factor affecting aggregate formation [27]. It may be due to the provision of moisture required by the soil. Adequate moisture facilitates microbial activity and organic matter decomposition, key to soil aggregate formation. Additionally, moisture promoted the bonding of soil particles, aiding in aggregate formation and stability. Furthermore, temperature affects microbial activity in the soil; optimal temperatures can enhance microbial growth and organic matter decomposition [28], which is beneficial for soil aggregate formation. Precipitation and temperature together influenced plant growth and root development, thereby affecting soil aggregate formation. Plant roots can promote the binding of soil particles, while the decomposition of plant residues provides organic matter, increasing soil structural stability. Previous studies have shown that different soil types (such as sand, loam, and clay) have varying physical and chemical properties, which also affect the binding capacity of soil particles [29]. Additionally, organic matter was one of the key factors in soil aggregate formation, with a high organic matter content contributing to enhanced soil structural stability [30].

In this study, we found that larger aggregates had a higher organic carbon content than smaller ones, consistent with previous research conclusions [31]. Large aggregates provided a microenvironment where organic matter was protected from microbial decomposition. This physical isolation reduced the chances of microbial contact with organic matter, slowing down the decomposition rate. The microenvironment in large aggregates was favorable for specific microbial communities that participate in the transformation and stabilization of organic matter. This microbial activity contributed to the accumulation of organic matter within aggregates. The growth of plant roots in soil leads to the secretion of organic substances that promote the formation of soil aggregates. Large aggregates often form in the rhizosphere; thus, they may contain higher levels of root exudates and, consequently, enriched organic carbon. Additionally, soil mineral particles and clay particles in large aggregates may have a strong adsorption capacity for organic matter, which helps to fix and retain organic carbon [32].

SOC mineralization is a crucial process in the balance of soil carbon pools and its study helps reveal the dynamics of soil carbon storage. The rate of mineralization indicates the speed of organic carbon decomposition. Overall, aggregates of different sizes exhibit a high rate of organic carbon mineralization in the initial stages of incubation, followed by a rapid decline. The mineralization rate slowed over time, becoming relatively stable, which was associated with soil microbial activity and the ease of carbon mineralization [33]. Organic carbon was decomposed quickly into less efficiently mineralizable parts; most organic carbon decomposed during 60 days of indoor incubation is the easily mineralizable type. Initially, soil and aggregate samples, moistened to 60% of field capacity, stimulated microbial activity. Easily mineralizable organic carbon, such as sugars and proteins, was abundant and rapidly decomposed by microbes, releasing large amounts of CO_2 . Over

time, as the readily available organic carbon was depleted, the rate of mineralization gradually decreased, showing a relatively stable trend. In this study, SOC mineralization in soil aggregates showed a highly significant positive correlation with precipitation ($p < 0.001$). Organic matter in soil aggregates, such as plant residues and dead microbial matter, were the primary materials for mineralization [34]. Precipitation provided the necessary moisture for the decomposition of this organic matter, thereby increasing the mineralization rate. Increased precipitation also alters soil oxygen exchange conditions. Appropriate moisture content facilitates oxygen penetration, providing the oxygen needed for the aerobic decomposition of organic carbon by soil microbes. Soil moisture conditions also indirectly affect soil temperature and chemical properties, which collectively influence the mineralization process of organic carbon. Furthermore, compared to other particle sizes, the 1–2 mm aggregates showed more excellent cumulative mineralization and are more closely related to MAP, SOC, and SWOC. It could be due to the size of 1–2 mm aggregates being more conducive to microbial activity and organic matter accumulation. The particle size provided a larger surface area for microbial contact with organic matter, while maintaining suitable moisture and gas exchange conditions, crucial for microbial metabolic activities. Precipitation, as a critical climatic factor, directly affects soil moisture conditions and microbial activity. The 1–2 mm aggregates under different precipitation conditions exhibited a more robust moisture retention capacity, thereby affecting the rate of mineralization and organic matter transformation. The organic matter content within aggregates, especially SOC and SWOC, directly influenced the mineralization process. The 1–2 mm aggregates, due to their specific physical structure, may more effectively retain and transform SOC and SWOC, thereby impacting the mineralization process.

4.2. Soil Organic Carbon and Its Mineralization

This study found that during a 60-day incubation period, the highest SOC content and cumulative mineralized carbon were observed in MS, followed by TS, with the lowest in DS. The reason for this outcome is that the MS region received higher rainfall, resulting in generally higher soil moisture content, which provided an optimal environment for microbial survival, thereby enhancing microbial activity. Active microbial communities can more effectively decompose and transform organic matter in the soil, accelerating the SOC mineralization process [35]. Additionally, ample rainfall not only supplies necessary moisture but also improves soil physical properties, such as soil porosity and structural stability. These improvements aided in increasing oxygen diffusion in the soil, providing conditions for aerobic decomposition of organic carbon. In areas with higher rainfall, plant growth was usually more vigorous, leading to increased organic matter inputs in the soil, such as fallen leaves and root exudates [36]. These inputs of organic matter provided more substrates for SOC mineralization. Areas with higher rainfall were often accompanied by specific climatic patterns, such as higher humidity and lower temperature fluctuations, which directly impacted the mineralization and stability of SOC [37].

We found that for profile soils, both the SOC content and its cumulative mineralization significantly decrease with increasing soil depth [38]. Typically, the topsoil had higher SOC content due to more abundant plant residues and root exudates, as well as a more active microbial community. As soil depth increases, the input of these organic materials diminishes and microbial activity decreases, resulting in relatively lower SOC content in the subsoil. The subsoil usually receives less organic matter, as most plant debris and organic wastes accumulate in the topsoil [39]. Microbial activity in the subsoil was generally lower than in the topsoil due to a limited supply of oxygen and moisture, which were essential for microbial growth and activity. Additionally, the temperature in the subsoil was usually lower than that of the topsoil. The cooler temperatures slowed down microbial activity, making the organic matter in the subsoil more stable and less susceptible to microbial decomposition, thereby reducing the rate of organic carbon mineralization.

Additionally, precipitation had a more significant impact on the mineralization of organic carbon in the topsoil than in the subsoil. The organic carbon mineralization in

the 0–50 cm soil layer showed a highly significant positive correlation with precipitation ($p < 0.001$), while in the 50–100 cm layer, it is highly significantly correlated with SOC and POC ($p < 0.001$). The reason for this may be that precipitation typically only affects soil layers ranging from a few centimeters to several tens of centimeters. In other cases, especially during prolonged heavy rains or in soils with good permeability, water can penetrate soil layers several meters deep. Precipitation directly increases the moisture content of the topsoil, providing necessary conditions for the survival and activity of soil microbes [40]. This increased moisture condition had a direct and significant promoting effect on the mineralization process of SOC, as microbial activity is the primary driver of SOC mineralization. In the subsoil, the sources and nature of SOC may differ from those in the topsoil. The SOC in the subsoil was more likely derived from harder-to-decompose organic matter, such as plant root residues, and its mineralization process was more closely related to soil POC [41]. Furthermore, Clay + Silt showed a significant positive correlation with SOC mineralization in the 50–100 cm soil layer ($p < 0.05$). In the subsoil, SOC mainly came from hard-to-decompose organic matter, such as deeper root residues. Silt and clay, due to their high water retention and adsorption capabilities, may more easily retain these hard-to-decompose organic matters, thus affecting SOC mineralization. Silt and clay had a high specific surface area and ion exchange capacity. These physical properties enable fine-grained soils to more effectively adsorb and retain organic matter, influencing SOC accumulation and mineralization to some extent. Silt and clay were often rich in minerals, such as iron and aluminum oxides, which can form stable complexes with organic matter, affecting the dynamics of SOC mineralization. This effect may be more pronounced in the subsoil.

5. Conclusions

The variation in soil aggregate size distribution along the precipitation gradient reflected the impact of environmental factors on soil structure. A more humid climate is conducive to the formation of larger soil aggregates. With increasing soil depth, the SOC content and cumulative mineralization decrease and the impact of precipitation on SOC mineralization gradually diminishes. Precipitation primarily controlled the SOC mineralization characteristics in the 0–50 cm soil layer, while in the 50–100 cm layer, SOC mineralization was more closely related to soil-associated carbon. Additionally, the distribution and cumulative mineralization of soil organic carbon in different grassland types of the Loess Plateau also decreased significantly with the reduction in precipitation gradient.

We concluded that in high precipitation areas, the turnover rate of SOC was faster compared to low precipitation areas, leading to an increase in CO₂ emissions into the atmosphere. In the scenario of global warming, these findings provided new insights into predicting the stability and response of soil organic carbon mineralization in grasslands to climate change and they were significant for maintaining the functionality of grassland soil ecosystems, plant growth, and the global carbon balance. In future research, more attention should be paid to the carbon dynamics of soils in high-precipitation areas and their interactions with climate.

Author Contributions: Z.Z. and N.H. jointly designed the research; C.G., M.L., B.F. and Y.Z. conducted the research; C.G. and Z.Z. wrote the manuscript; N.H. and J.Z. commented. All authors have read and agreed to the published version of the manuscript.

Funding: This work was supported by the Second Tibetan Plateau Scientific Expedition and Research Program (2019QZKK0606-2) and the International Cooperation Project of Science and Technology Department of Jilin Province, China (20220402061GH).

Institutional Review Board Statement: Not applicable.

Informed Consent Statement: Not applicable.

Data Availability Statement: The data presented in this study are available upon request from the corresponding author. The data are not publicly available due to laboratory regulations.

Conflicts of Interest: The authors declare no conflicts of interest.

References

- Hungate, B.A.; Groenigen, K.J.V.; Six, J.; Jastrow, J.D.; Luo, Y.; Graaff, M.A.D.; Osenberg, C.W. Assessing the effect of elevated carbon dioxide on soil carbon: A comparison of four meta-analyses. *Glob. Chang. Biol.* **2009**, *15*, 2020–2034. [[CrossRef](#)]
- Čeh-Brežnik, B.; Tajnšek, A. Distribution of nitrogen in wheat plant in its late growth stages with regard to organic fertilisation and mineral nitrogen rate. *Plant Soil Environ.* **2006**, *51*, 553–561. [[CrossRef](#)]
- Yang, S.; Zhang, Z.; Cong, L.; Wang, X.; Shi, S. Effect of fulvic acid on the phosphorus availability in acid soil. *J. Soil Sci. Plant Nutr.* **2013**, *13*, 526–533. [[CrossRef](#)]
- Fageria, N.K.; Baligar, V.C.; Li, Y.C. The Role of Nutrient Efficient Plants in Improving Crop Yields in the Twenty First Century. *J. Plant Nutr.* **2008**, *31*, 1121–1157. [[CrossRef](#)]
- Mi, J.; Li, J.J.; Chen, D.M.; Xie, Y.C.; Bai, Y.F. Predominant control of moisture on soil organic carbon mineralization across a broad range of arid and semiarid ecosystems on the Mongolia plateau. *Landsc. Ecol.* **2015**, *30*, 1683–1699. [[CrossRef](#)]
- Wu, Z.T.; Dijkstra, P.; Koch, G.W.; Peñuelas, J.; Hungate, B.A. Responses of terrestrial ecosystems to temperature and precipitation change: A meta-analysis of experimental manipulation. *Glob. Chang. Biol.* **2011**, *17*, 927–942. [[CrossRef](#)]
- Kpemoua, T.P.I.; Barre, P.; Chevallier, T.; Houot, S.; Chenu, C. Drivers of the amount of organic carbon protected inside soil aggregates estimated by crushing: A meta-analysis. *Geoderma* **2022**, *427*, 116089. [[CrossRef](#)]
- Qu, J.F.; Tan, M.; Hou, Y.L.; Ge, M.Y.; Chen, F. Effects of the stability of reclaimed soil aggregates on organic carbon in coal mining subsidence areas. *Appl. Eng. Agric.* **2018**, *34*, 843–854. [[CrossRef](#)]
- Magnusson, T. Studies of the soil atmosphere and related physical site characteristics in mineral forest soils. *Eur. J. Soil Sci.* **2010**, *43*, 767–790. [[CrossRef](#)]
- Song, W.; Zhao, B.; Mu, C.C.; Ballikaya, P.; Cherubini, P.; Wang, X. Moisture availability influences the formation and characteristics of earlywood of *Pinus tabuliformis* more than latewood in northern China. *Agric. Forest Meteorol.* **2022**, *327*, 109219. [[CrossRef](#)]
- Wu, Y.Y.; Ouyang, W.; Hao, Z.C.; Lin, C.Y.; Liu, H.B.; Wang, Y.D. Assessment of soil erosion characteristics in response to temperature and precipitation in a freeze-thaw watershed. *Geoderma* **2018**, *328*, 56–65. [[CrossRef](#)]
- Wordell-Dietrich, P.; Wotte, A.; Rethemeyer, J.; Bachmann, J.; Helfrich, M.; Kirfel, K.; Leuschner, C.; Don, A. Vertical partitioning of CO₂ production in a forest soil. *Biogeosciences* **2020**, *17*, 6341–6356. [[CrossRef](#)]
- Azam, A.; Akhtar, M.S.; Rukh, S.; Mehmood, A.; Imran, M.; Khan, A.; Qayyum, A.; Ahmad, W.; Gurmani, A.R. Changes in Soil Organic Carbon Fractions Across a Loess Toposequence. *J. Soil Sci. Plant Nutr.* **2020**, *20*, 1193–1202. [[CrossRef](#)]
- Li, J.; Pei, J.; Pendall, E.; Reich, P.B.; Noh, N.J.; Li, B.; Fang, C.; Nie, M. Rising temperature may trigger deep soil carbon loss across forest ecosystems. *Adv. Sci.* **2020**, *7*, 2001242. [[CrossRef](#)] [[PubMed](#)]
- Li, Y.; Wang, T.; Camps-Arbestain, M.; Whitby, C.P. The regulators of soil organic carbon mineralization upon lime and/or phosphate addition vary with depth. *Sci. Total Environ.* **2022**, *828*, 154378. [[CrossRef](#)] [[PubMed](#)]
- Vormstein, S.; Kaiser, M.; Piepho, H.P.; Joergensen, R.G.; Ludwig, B. Effects of fine root characteristics of beech on carbon turnover in the topsoil and subsoil of a sandy Cambisol. *Eur. J. Soil Sci.* **2017**, *68*, 177–188. [[CrossRef](#)]
- Bukombe, B.; Fiener, P.; Hoyt, A.M.; Doetterl, S. Controls on heterotrophic soil respiration and carbon cycling in geochemically distinct African tropical forest soils. *Soil* **2021**, *7*, 639–659. [[CrossRef](#)]
- Sasaki, A.; Hagimori, Y.; Nakatsubo, T.; Hoshika, A. Tidal effects on the organic carbon mineralization rate under aerobic conditions in sediments of an intertidal estuary. *Ecol. Res.* **2009**, *24*, 937–941. [[CrossRef](#)]
- Cui, L.L.; Li, X.; Lin, J.; Guo, G.; Zhang, X.; Zeng, G.R. The mineralization and sequestration of soil organic carbon in relation to gully erosion. *CATENA* **2022**, *214*, 106218. [[CrossRef](#)]
- Kan, Z.R.; Ma, S.T.; Liu, Q.Y.; Liu, B.Y.; Virk, A.L.; Qi, J.Y.; Zhao, X.; Lal, R.; Zhang, H.L. Carbon sequestration and mineralization in soil aggregates under long-term conservation tillage in the North China Plain. *CATENA* **2020**, *188*, 104428. [[CrossRef](#)]
- Kan, Z.R.; Virk, A.L.; He, C.; Liu, Q.Y.; Qi, J.Y.; Dang, Y.P.; Zhao, X.; Zhang, H.L. Characteristics of carbon mineralization and accumulation under long-term conservation tillage. *CATENA* **2020**, *193*, 104636. [[CrossRef](#)]
- Cambardella, C.A.; Elliott, E.T. Particulate soil organic-matter changes across a grassland cultivation sequence. *Soil Sci. Soc. Am. J.* **1992**, *56*, 777–783. [[CrossRef](#)]
- Bowman, R.A.; Reeder, J.D.; Wienhold, B.J. Quantifying laboratory and field variability to assess potential for carbon sequestration. *Commun. Soil Sci. Plant Anal.* **2002**, *33*, 1629–1642. [[CrossRef](#)]
- Chen, Y.; Huang, Y.; Sun, W.J. Using Organic Matter and pH to Estimate the Bulk Density of Afforested/Reforested Soils in Northwest and Northeast China. *Pedosphere* **2017**, *27*, 890–900. [[CrossRef](#)]
- Jia, J.; Yu, D.P.; Zhou, W.M.; Zhou, L.; Bao, Y.; Meng, Y.Y.; Dai, L.M. Variations of Soil Aggregates and Soil Organic Carbon Mineralization across Forest Types on the Northern Slope of Changbai Mountain. *Acta Ecol. Sin.* **2015**, *35*, 1–7. [[CrossRef](#)]
- Robertson, G.P.; Wedin, D.; Groffman, P.M.; Blair, J.M.; Holland, E.A.; Nadelhoffer, K.J.; Harris, D. Soil Carbon and Nitrogen Availability Nitrogen Mineralization, Nitrification and Soil Respiration Potentials. In *Standard Soil Methods for Long-Term Ecological Research*; Academic Press: Cambridge, MA, USA, 1999; pp. 258–271. [[CrossRef](#)]
- Cui, Y.Y.; Hou, D.J.; Wang, Z.W.; Wang, J.; Qu, Z.Q.; Wang, Y.B.; Han, G.D.; Li, Z.G.; Ren, H.Y.; Wang, H.M. Responses of soil aggregate stability to carbon and nitrogen under precipitation gradients in a desert steppe. *J. Soils Sediments* **2024**, *24*, 1071–1081. [[CrossRef](#)]

28. Yan, G.Y.; Xing, Y.J.; Wang, J.Y.; Zhang, Z.; Xu, L.; Han, S.; Zhang, J.H.; Dai, G.H.; Wang, Q.G. Effects of winter snowpack and nitrogen addition on the soil microbial community in a temperate forest in northeastern China. *Ecol. Indic.* **2018**, *93*, 602–611. [[CrossRef](#)]
29. Dai, S.S.; Li, L.J.; Ye, R.; Zhu-Barker, X.; Horwath, W.R. The temperature sensitivity of organic carbon mineralization is affected by exogenous carbon inputs and soil organic carbon content. *Eur. J. Soil Biol.* **2017**, *81*, 69–75. [[CrossRef](#)]
30. Lockwood, P.V.; Rabbi, S.M.; Wilson, B.R.; Danile, H.; Young, I.M. Soil organic carbon mineralization rates in aggregates under contrasting land uses. *Geoderma* **2014**, *216*, 10–18. [[CrossRef](#)]
31. Zhao, Z.H.; Mao, Y.L.; Gao, S.F.; Lu, C.Y.; Pan, C.J.; Li, X.Y. Organic carbon accumulation and aggregate formation in soils under organic and inorganic fertilizer management practices in a rice–wheat cropping system. *Sci. Rep.* **2023**, *13*, 3665. [[CrossRef](#)]
32. Suetsugu, A.; Sato, T.; Kaneta, Y.; Sato, A. Effects of Organo-mineral Complexes on Flocculation, Settlement and Vertical Distribution of Bioelements in Soil Suspensions. *J. Soil Sci. Plant Nutr.* **2005**, *51*, 323–331. [[CrossRef](#)]
33. Yu, H.; Sui, Y.Y.; Chen, Y.M.; Bao, T.L.; Jiao, X.G. Soil Organic Carbon Mineralization and Its Temperature Sensitivity under Different Substrate Levels in the Mollisols of Northeast China. *Life* **2022**, *12*, 712. [[CrossRef](#)] [[PubMed](#)]
34. Tardy, V.; Spor, E.; Mathieu, O.; Eque, J.L.E.; Maron, P.A. Shifts in microbial diversity through land use intensity as drivers of carbon mineralization in soil. *Soil Boil. Biochem.* **2015**, *90*, 204–213. [[CrossRef](#)]
35. Chai, H.; Li, J.; Ochoa-Hueso, R.; Yang, X.C.; Li, J.Q.; Meng, B.; Song, W.Z.; Zhong, X.Y.; Ma, J.Y.; Sun, W. Different drivers of soil C accumulation in aggregates in response to altered precipitation in a semiarid grassland. *Sci. Total Environ.* **2022**, *830*, 154760. [[CrossRef](#)] [[PubMed](#)]
36. Chen, X.M.; Zhang, D.Q.; Liang, G.H.; Qiu, Q.Y.; Liu, J.X.; Zhou, G.Y.; Liu, S.Z.; Chu, G.W.; Yan, J.H. Effects of precipitation on soil organic carbon fractions in three subtropical forests in southern China. *J. Plant Ecol.* **2015**, *9*, 10–19. [[CrossRef](#)]
37. Zhang, Y.; Li, P.; Liu, X.J.; Xiao, L.; Li, T.B.; Wang, D.J. The response of soil organic carbon to climate and soil texture in China. *Front. Earth Sci.* **2022**, *16*, 835–845. [[CrossRef](#)]
38. Mishra, G.; Gorai, A.K. Horizontal and vertical profiling of soil organic carbon stock in Nagaland, North East India. *Curr. Sci. India* **2022**, *119*, 25. [[CrossRef](#)]
39. Wu, Y.J.; Wang, F.Y.; Zhu, S.X. Vertical distribution characteristics of soil organic carbon content in Caohai wetland ecosystem of Guizhou plateau, China. *J. For. Res.* **2016**, *27*, 551–556. [[CrossRef](#)]
40. Wilhelm, R.C.; Lynch, L.; Webster, T.M.; Schweizer, S.; Inagaki, T.M.; Tfaily, M.M.; Kukkadapu, R.; Hoeschen, C.; Buckley, D.H.; Lehmann, J. Susceptibility of new soil organic carbon to mineralization during dry-wet cycling in soils from contrasting ends of a precipitation gradient. *Soil Boil. Biochem.* **2022**, *169*, 108681. [[CrossRef](#)]
41. Xu, G.; Song, J.; Zhang, Y.; Lv, Y. Effects of biochar application on soil organic carbon mineralization during drying and rewetting cycles. *BioResources* **2019**, *14*, 9957–9967. [[CrossRef](#)]

Disclaimer/Publisher’s Note: The statements, opinions and data contained in all publications are solely those of the individual author(s) and contributor(s) and not of MDPI and/or the editor(s). MDPI and/or the editor(s) disclaim responsibility for any injury to people or property resulting from any ideas, methods, instructions or products referred to in the content.